

# Atmospheric neutrinos with three flavor mixing

Mohan Narayan, G. Rajasekaran

*Institute of Mathematical Sciences, Madras 600 113, India.*

S. Uma Sankar

*Department of Physics, I.I.T., Powai, Bombay 400 076, India.*

(December 2, 2024)

## Abstract

We analyze the atmospheric neutrino data in the context of three flavor neutrino oscillations taking account of the matter effects in the earth. With the hierarchy among the vacuum mass eigenvalues  $\mu_3^2 \gg \mu_2^2 \geq \mu_1^2$ , the solution of the atmospheric neutrino problem depends on  $\delta_{31} = \mu_3^2 - \mu_1^2$  and the 13 and 23 mixing angles  $\phi$  and  $\psi$ . Whereas the sub-GeV atmospheric neutrino data imposes only a lower limit on  $\delta_{31} > 10^{-3} \text{ eV}^2$ , the zenith angle dependent suppression observed in the multi-GeV data limits  $\delta_{31}$  from above also. The allowed regions of the parameter space are strongly constrained by the multi-GeV data. Combined with our earlier solution to the solar neutrino problem which depends on  $\delta_{21} = \mu_2^2 - \mu_1^2$  and the 12 and 13 mixing angles  $\omega$  and  $\phi$ , we have obtained the ranges of values of the five neutrino parameters which solve both the solar and the atmospheric neutrino problems simultaneously.

## I. INTRODUCTION

In recent years, deep underground detectors have been measuring the flux of neutrinos produced in the atmosphere. (Unless explicitly stated, we call neutrinos and anti-neutrinos collectively as neutrinos). These neutrinos are produced from the decays of  $\pi^\pm$  and  $K^\pm$  which, in turn, are produced by cosmic ray interactions with the atmosphere. One expects the number of muon neutrinos to be twice the number of electron neutrinos. The predictions of detailed Monte Carlo calculations confirm that the ratio of the flux of muon neutrinos  $\Phi_{\nu_\mu}$  to the flux of electron neutrinos  $\Phi_{\nu_e}$  is about 2 [1,2]. The predicted neutrino fluxes from different calculations differ significantly from each other (by as much as 30%), but the predictions for the ratio of the fluxes  $\Phi_{\nu_\mu}/\Phi_{\nu_e}$  are in good agreement with each other. The large water Cerenkov detectors Kamiokande and IMB [3] have measured this ratio and have found it to be about half of what is predicted. The experimental results are presented in the form of a double ratio

$$R = \frac{\left(\frac{N_{\nu_\mu}}{N_{\nu_e}}\right)_{obs}}{\left(\frac{N_{\nu_\mu}}{N_{\nu_e}}\right)_{MC}} = \frac{r_{obs}}{r_{MC}}. \quad (1)$$

Kamiokande collaboration have presented their results for neutrinos with energy less than 1.33 GeV (sub-GeV data) [4] and for neutrinos with energy greater than 1.33 GeV (multi-GeV data) [5]. For the sub-GeV data,  $R = 0.60^{+0.07}_{-0.06} \pm 0.05$  and for the multi-GeV data, after averaging over the zenith angle,  $R = 0.57^{+0.08}_{-0.07} \pm 0.07$ . The value of  $R$  has no significant zenith angle dependence for the sub-GeV data. However, for the multi-GeV data,  $R$  is smaller for large values of zenith angle (upward going neutrinos) and is larger for small values of zenith angle (downward going neutrinos). Kamiokande have analyzed their data assuming that the smaller observed value of  $R$  is caused by neutrino oscillations. They have done two independent analyses, one assuming two flavor oscillations between  $\nu_\mu \leftrightarrow \nu_e$  and the other assuming two flavor oscillations between  $\nu_\mu \leftrightarrow \nu_\tau$ . For both the cases, they obtain a mass-squared difference  $\delta m^2 \sim 10^{-2} eV^2$  and a mixing angle nearly  $45^0$ . Since the upward going neutrinos travel large distances inside the earth before entering the detector, matter

effects may be important for these, especially at higher energies. Therefore one must take matter effects into consideration while analyzing  $\nu_\mu \leftrightarrow \nu_e$  oscillations. These matter effects may be able to explain the observed zenith angle dependence in the multi-GeV data.

Atmospheric neutrino problem was analyzed in the three flavor neutrino oscillation framework previously. In Ref. [6] the sub-GeV data were analyzed under the assumption that one of the mass differences is much smaller than the other. The matter effects due to the passage of neutrinos through the earth were included and the allowed values of neutrino parameters were obtained. Various other authors have analyzed, in the context of three flavor oscillations, accelerator and reactor data in conjunction with the sub-GeV atmospheric data [7] or the multi-GeV data with zenith angle dependence included [8]. However, in both these cases the earth matter effects were not taken into account.

Several authors have attempted a simultaneous solution of the solar and atmospheric neutrino problems in three flavor oscillation scenarios. The solution in Ref. [9] assumes maximal mixing between all the three flavors and derives the constraints on the mass differences. The solution thus obtained restricts the mass difference to be very small ( $\sim 10^{-10} \text{ eV}^2$ ) and is somewhat fine-tuned. Other solutions have assumed the mass hierarchy that was considered in Ref. [6] and obtained the allowed regions in the neutrino parameter space [10–13]. However, all these analyses were based mostly on the sub-GeV atmospheric neutrino data. The earth matter effects and the zenith angle dependence of the multi-GeV data were not taken into account. In a recent analysis of the multi-GeV data both the matter effects and the zenith angle dependence were taken into account [14]. However, this analysis considered the atmospheric neutrino problem only.

In this paper, we analyze the Kamiokande multi-GeV data in the framework of three flavor neutrino oscillations. The solar neutrino data and the sub-GeV data of Kamiokande were analyzed earlier in the same framework [13]. We only assume that, of the two mass differences in the problem, the smaller one is chosen to solve the solar neutrino problem and the larger one will be relevant for the atmospheric neutrino problem. We do not, *apriori*, make any assumption about the form of the mixing matrix. Our starting point is the same

as that in Ref. [6]. We include the matter effects due to the passage of neutrinos through the earth. We take the allowed values of neutrino parameters from our earlier work as inputs. The zenith angle dependent suppression of multi-GeV data places strong further constraints on the parameter space allowed by the solar neutrino problem and the sub-GeV atmospheric neutrino data. In section II, we define our theoretical framework and derive the oscillation probabilities. In section III, we describe the comparison of the theoretical predictions with the Kamiokande data and determine the allowed regions of the neutrino parameters. In section IV we discuss our results and present our conclusions. A brief discussion of the recent LSND result [15] is also included.

## II. THEORY

Here we describe the three flavor neutrino mixing and calculate the probability for a neutrino produced as  $\nu_\alpha$  to be detected as  $\nu_\beta$ , where  $\alpha$  and  $\beta$  are flavor indices. The flavor eigenstates are related to the mass eigenstates by

$$\begin{bmatrix} \nu_e \\ \nu_\mu \\ \nu_\tau \end{bmatrix} = U^v \begin{bmatrix} \nu_1^v \\ \nu_2^v \\ \nu_3^v \end{bmatrix} \quad (2)$$

where the superscript ‘v’ denotes vacuum. The unitary matrix  $U^v$  can be parametrized as

$$U^v = U^{phase} \times U^{23}(\psi) \times U^{13}(\phi) \times U^{12}(\omega), \quad (3)$$

where  $U^{ij}(\theta_{ij})$  is the two flavor mixing matrix between the  $i$ th and  $j$ th mass eigenstates with the mixing angle  $\theta_{ij}$ . For simplicity, we neglect the CP violation and set  $U^{phase} = I$ .

In the mass basis the mass-squared matrix is diagonal and can be taken to be

$$M_0^2 = \begin{bmatrix} \mu_1^2 & 0 & 0 \\ 0 & \mu_2^2 & 0 \\ 0 & 0 & \mu_3^2 \end{bmatrix} = \mu_1^2 I + \begin{bmatrix} 0 & 0 & 0 \\ 0 & \delta_{21} & 0 \\ 0 & 0 & \delta_{31} \end{bmatrix}, \quad (4)$$

where  $\delta_{21} = \mu_2^2 - \mu_1^2$  and  $\delta_{31} = \mu_3^2 - \mu_1^2$ . Without loss of generality we can take  $\mu_3 > \mu_2 > \mu_1$  so that both  $\delta_{21}$  and  $\delta_{31}$  are positive. For extreme relativistic neutrinos, the oscillation probability depends only on the mass-squared differences so we ignore the first term  $\mu_1^2 I$ .

In the flavor basis, the mass-squared matrix is non-diagonal and is given by

$$M_v^2 = U^v M_0^2 (U^v)^\dagger. \quad (5)$$

For the propagation of neutrinos through the earth, we need to take the matter effects into account. The charged current scattering between electrons and  $\nu_e$  induces an effective mass-squared term for  $\nu_e$  which is of the form  $A = 2\sqrt{2}G_F N_e E$ , where  $N_e$  is the number density of electrons and  $E$  is the neutrino energy [16]. This term is present only for the  $e - e$  element in the flavor basis so the mass-squared matrix including the matter effects is

$$M_m^2 = M_v^2 + \begin{bmatrix} A & 0 & 0 \\ 0 & 0 & 0 \\ 0 & 0 & 0 \end{bmatrix}. \quad (6)$$

$M_m^2$  is a hermitian matrix and can be diagonalized by unitary matrix  $U^m$ , which relates the flavor eigenstates to matter dependent mass eigenstates

$$\begin{bmatrix} \nu_e \\ \nu_\mu \\ \nu_\tau \end{bmatrix} = U^m \begin{bmatrix} \nu_1^m \\ \nu_2^m \\ \nu_3^m \end{bmatrix} \quad (7)$$

where the superscript ‘m’ stands for matter. We denote the matter dependent mass eigenvalues as  $m_1$ ,  $m_2$  and  $m_3$ . The matter dependent mixing matrix  $U^m$  can be parametrized in terms of three mixing angles in a manner similar to that of  $U^v$  as given in eq.(3). The matter dependent mass eigenvalues and mixing angles can be obtained, in terms of the vacuum parameters and  $A$ , by solving the eigenvalue problem of  $M_m^2$  in eq.(6)

The distance scales and the energy scales in the solar neutrino problem and the atmospheric neutrino problem are very different. Therefore, one needs two distinct mass scales to solve the solar and the atmospheric neutrino problems simultaneously. To satisfy the

constraints from all the three solar neutrino experiments, one must choose  $\delta_{21} \sim 10^{-5} \text{ eV}^2$ , which is roughly the matter term  $A$  for the solar neutrinos due to their passage through the sun. As we will shortly see, the sub-GeV atmospheric neutrino data impose a constraint  $\delta_{31} \geq 10^{-3} \text{ eV}^2$ . Hence  $\delta_{31} \gg \delta_{21}$ . If  $\delta_{21} \sim 10^{-5} \text{ eV}^2$ , the oscillation length corresponding to it, even for the minimum of the atmospheric neutrino energies, is of the order of the diameter of the earth. In the expression for the oscillation probability,  $\delta_{21}$  can be set to zero. Therefore the oscillations are dependent on only one mass difference  $\delta_{31}$  in the atmospheric neutrino problem.

In the approximation of neglecting  $\delta_{21}$ , it is straightforward to show that the oscillation probability is independent of the mixing angle  $\omega$ . Including matter effects does not alter this conclusion. Note, however, that neglecting  $\delta_{21}$  does not reduce the problem to an effective two flavor mixing. The three flavor nature of the problem is reflected by the fact that the oscillation probability is a function of the mass difference  $\delta_{31}$  and *two* mixing angles  $\phi$  and  $\psi$ . In the case of an effective two flavor mixing, the oscillation probability is dependent on one mixing angle only. When the matter effects are included the mixing angle  $\psi$  remains unaffected but the angle  $\phi$  becomes matter dependent [6],

$$\tan 2\phi_m = \frac{\delta_{31} \sin 2\phi}{\delta_{31} \cos 2\phi - A}. \quad (8)$$

The mass eigenvalue of  $\nu_1^m$  remains 0 (actually it is of the order of  $\delta_{21}$  which we are neglecting here). The other two matter dependent mass eigenvalues are given by

$$m_2^2 = \frac{1}{2} \left[ (\delta_{31} + A) - \sqrt{(\delta_{31} \cos 2\phi - A)^2 + (\delta_{31} \sin 2\phi)^2} \right] \quad (9)$$

$$m_3^2 = \frac{1}{2} \left[ (\delta_{31} + A) + \sqrt{(\delta_{31} \cos 2\phi - A)^2 + (\delta_{31} \sin 2\phi)^2} \right] \quad (10)$$

Equations (8), (9) and (10) are valid for neutrinos. For anti-neutrinos, we get a similar set of formulae with  $A$  replaced by  $-A$ .

The neutrinos produced in the atmosphere enter the earth after travelling through the atmosphere for about 20 Km and finally reach the detector after travelling through the earth. The distance travelled through the earth is a function of the zenith angle. For the

five bins considered by Kamiokande [5], the average values of the cosine of the zenith angle are  $-0.8, -0.4, 0.0, 0.4, 0.8$  and the average distances travelled through the earth are  $10210, 5137, 832, 34, 6$  Km respectively [9].

A neutrino of flavor  $\alpha$ , produced in the atmosphere at time  $t = 0$ , propagates through the atmosphere as a linear combination of the vacuum mass eigenstates. If the neutrino enters earth at time  $t = t_1$ , its state vector at that time can be written as

$$|\Psi_\alpha(t_1)\rangle = \sum_i U_{\alpha i}^v \exp\left(-i\frac{\mu_i^2 t_1}{2E}\right) |\nu_i^v\rangle. \quad (11)$$

Reexpressing the vacuum mass eigenstates in terms of flavor states, we have

$$|\Psi_\alpha(t_1)\rangle = \sum_i U_{\alpha i}^v \exp\left(-i\frac{\mu_i^2 t_1}{2E}\right) \sum_\lambda U_{\lambda i}^{v*} |\nu_\lambda\rangle. \quad (12)$$

After entering the earth, the neutrino propagates as a linear combination of the matter dependent mass eigenstates. We take the earth to be a slab of constant density. At the time of detection  $t = t_d$ , the state vector takes the form

$$|\Psi_\alpha(t_d)\rangle = \sum_i U_{\alpha i}^v \exp\left(-i\frac{\mu_i^2 t_1}{2E}\right) \sum_\lambda U_{\lambda i}^{v*} \sum_j U_{\lambda j}^m \exp\left(-i\frac{m_j^2(t_d - t_1)}{2E}\right) |\nu_j^m\rangle. \quad (13)$$

Hence the amplitude for the neutrino produced as flavor  $\alpha$  at  $t = 0$  to be detected as a neutrino of flavor  $\beta$  at time  $t_d$  is given by

$$\langle \nu_\beta | \Psi_\alpha(t_d) \rangle = \sum_i \sum_\lambda \sum_j U_{\alpha i}^v U_{\lambda i}^{v*} U_{\lambda j}^m U_{\beta j}^{m*} \exp\left(-i\frac{\mu_i^2 t_1}{2E}\right) \exp\left(-i\frac{m_j^2(t_d - t_1)}{2E}\right). \quad (14)$$

The probability of oscillation  $P_{\alpha\beta}$  is given by the modulus square of the above amplitude. If  $t_d - t_1$  is set equal to zero (that is if the total time of travel is equal to the time of travel through the atmosphere) then the expression in eq.(14) reduces to the simple vacuum oscillation amplitude. The same is true if the matter effects are ignored; i.e. if  $U^m = U^v$  and  $m_i = \mu_i$ .

For bins 1, 2 and 3, the distance travelled in earth is much larger than the distance travelled in the atmosphere. Therefore  $t_1$  is much smaller than  $t_d$  for these bins and can be neglected. Neglecting  $t_1$ , simplifies the expressions for oscillation probability and we obtain

the expressions derived earlier in Ref. [6]. However, for bins 4 and 5, the distance of travel in atmosphere is comparable to that in earth. Therefore  $t_1$  is of the same of order of magnitude as  $t_d$  and can not be neglected. Keeping  $t_1 \neq 0$  in eq.(14) properly takes into account the non-adiabaticity in the abrupt change in density when the neutrino enters earth.

### III. CALCULATION AND RESULTS

#### A. Sub-GeV Data

First we briefly describe our analysis of the sub-GeV data and highlight the contrast between it and the analysis of the multi-GeV data. Matter effects are unimportant for the sub-GeV data. If the earth is taken to be a slab of density  $5.5 \text{ gm/cm}^3$ , the matter term  $A$  for the sub-GeV neutrinos is less than  $3.8 \times 10^{-4} \text{ eV}^2$ . As we will shortly see, the sub-GeV data sets a lower limit on  $\delta_{31} > 10^{-3} \text{ eV}^2$ . Hence the matter effects can be neglected and the expressions for  $P_{\alpha\beta}$  in the sub-GeV analysis are simply the vacuum oscillation probabilities

$$\begin{aligned} P_{\alpha\beta}^0 = & \left( U_{\alpha 1}^v U_{\beta 1}^v \right)^2 + \left( U_{\alpha 2}^v U_{\beta 2}^v \right)^2 + \left( U_{\alpha 3}^v U_{\beta 3}^v \right)^2 + \\ & 2 U_{\alpha 1}^v U_{\alpha 2}^v U_{\beta 1}^v U_{\beta 2}^v \cos \left( 2.53 \frac{d \delta_{21}}{E} \right) + \\ & 2 U_{\alpha 1}^v U_{\alpha 3}^v U_{\beta 1}^v U_{\beta 3}^v \cos \left( 2.53 \frac{d \delta_{31}}{E} \right) + \\ & 2 U_{\alpha 2}^v U_{\alpha 3}^v U_{\beta 2}^v U_{\beta 3}^v \cos \left( 2.53 \frac{d \delta_{32}}{E} \right), \end{aligned} \quad (15)$$

where  $d$  is the distance of travel in meters,  $\delta$ 's are the mass differences in  $\text{eV}^2$  and  $E$  is the neutrino energy in MeV. Because we have neglected the CP violating phase, the oscillation probability for the anti-neutrinos is the same as that for the neutrinos. Since  $\delta_{21}$  is very small, the cosine term containing it in eq.(15) can be set equal to 1. The other two cosine terms are dependent on  $\delta_{31}$  (and  $\delta_{32} \simeq \delta_{31}$ ), the neutrino energy and the distance of travel which is related to the zenith angle. As mentioned earlier, the double ratio  $R$  defined in eq.(1) does not have any zenith angle dependence for the sub-GeV data. One can account for this if it is possible to replace the distance dependent terms in eq.(15) by their average values.

This replacement is possible only if the average distance travelled contains many oscillation lengths. The above condition sets a lower limit on the mass difference  $\delta_{31} > 10^{-3} \text{ eV}^2$  [13]. Note that this lower limit is consistent with the approximation  $\delta_{31} \gg \delta_{21} \sim 10^{-5} \text{ eV}^2$ , which was made so that both solar and atmospheric neutrino problems could be solved simultaneously.

$P_{\alpha\beta}^0$  become independent of  $\delta_{31}$  and the neutrino energy when the distance dependent terms are replaced by their average values. They are simply functions of the mixing angles  $\phi$  and  $\psi$  alone. In this approximation, the expression for the double ratio  $R$  can be written as [13]

$$R = \frac{P_{\mu\mu}^0 + \frac{1}{r_{MC}} P_{e\mu}^0}{P_{ee}^0 + r_{MC} P_{\mu e}^0}, \quad (16)$$

where  $r_{MC}$  is the Monte Carlo expectation of the ratio of number  $\mu$ -like events to the number of  $e$ -like events. From the sub-GeV data of Kamiokande, we find  $r_{MC} = 1.912$  and  $R = 0.60_{-0.06}^{+0.07} \pm 0.05$  [4,13]. We take the allowed values of  $\phi$  from our analysis of solar neutrino data. The region of the parameter space which satisfies  $1\sigma$  experimental constraints restricts  $\phi$  to be in the range  $0 \leq \phi \leq 40^0$  [13]. We find the allowed region in the  $\phi - \psi$  plane by requiring the theoretical value calculated from eq.(16) to be within  $1\sigma$  or  $1.6\sigma$  uncertainty of the experimental value. In our previous analysis we restricted the range of  $\psi$  to be  $0 \leq \psi \leq 45^0$ . However, given the assumptions we made about vacuum mass eigenvalues, the most general possibility is to allow  $\psi$  to vary between 0 and  $90^0$  [17]. The new region allowed by the sub-GeV data, where  $\phi$  was restricted by the solar neutrino data and  $\psi$  is allowed to vary between 0 to  $90^0$ , is shown in Figure 1. The region between the solid lines is the parameter space which satisfies the experimental constraints at  $1\sigma$  level whereas the region between dashed lines satisfies the experimental constraints at  $1.6\sigma$  level. One important point to be noted in this analysis is that the sub-GeV data place only lower bound on  $\delta_{31}$ . Further the allowed region in  $\phi - \psi$  plane is quite large. In particular, the value  $\phi = 0$  is allowed at  $1\sigma$  level. This situation is to be contrasted with the bounds we get from multi-GeV data.

## B. Multi-GeV data

The multi-GeV data of Kamiokande have been presented for five zenith angle bins in Ref. [5]. For each of these bins, the observed numbers of electron-like events and muon-like events and their Monte Carlo expectations (without neutrino oscillations) have been given. From these one can calculate two sets of ratios

$$r_{MC}^i = \left( \frac{N_\mu^i}{N_e^i} \right)_{MC} \quad (17)$$

$$r_{obs}^i = \left( \frac{N_\mu^i}{N_e^i} \right)_{obs}, \quad (18)$$

and the set of double ratios

$$R^i = r_{obs}^i / r_{MC}^i \quad (19)$$

for each bin  $i = 1, 2, \dots, 5$ . We summarize the multi-GeV data of Kamiokande [5] in Table I. Note that  $r_{MC}^i$  are symmetric about  $\cos \theta = 0$ . This is a consequence of the fact that the atmospheric neutrino fluxes are symmetric about  $\cos \theta = 0$ .

The expected number of  $\mu$ -like and  $e$ -like events, in the absence of neutrino oscillations, is given by

$$N_\mu^i|_{N.O.} = \int \phi_{\nu_\mu}^i(E) \sigma_\mu dE + \int \phi_{\bar{\nu}_\mu}^i(E) \sigma_{\bar{\mu}} dE \quad (20)$$

$$N_e^i|_{N.O.} = \int \phi_{\nu_e}^i(E) \sigma_e dE + \int \phi_{\bar{\nu}_e}^i(E) \sigma_{\bar{e}} dE \quad (21)$$

where  $\phi$ 's are the fluxes of the atmospheric neutrinos at the location of Kamiokande. These are tabulated in Ref. [1] as functions of the neutrino energy (from  $E = 1.6$  GeV to  $E = 100$  GeV) and the zenith angle.  $\sigma_\mu$  and  $\sigma_{\bar{\mu}}$  are the charged current cross sections of  $\nu_\mu$  and  $\bar{\nu}_\mu$  respectively with nucleons. The crosssection is the sum of the quasi-elastic scattering and the deep inelastic scattering (DIS). The values for quasi-elastic scattering are taken from Gaisser and O'Connel [18] and those for the DIS are taken from Gargamelle data [19]. In calculating the DIS cross section, we took the lepton energy distribution to be given by the scaling formula (which is different for neutrinos and anti-neutrinos) and integrated

$d\sigma/dE_{lep}$  from the minimum lepton energy  $E_{min} = 1.33$  GeV to the maximum lepton energy  $E_{max} = E_\nu - m_\pi$ . The maximum lepton energy is chosen by defining DIS to contain at least one pion in addition to the charged lepton and the baryon.

The sample of  $\mu$ -like events are divided into fully contained (FC) and partially contained (PC) events whereas all the  $e$ -like events are fully contained. From figure 2(e) of Ref. [5] we see that all the fully contained  $\mu$ -like events are caused by neutrinos with energy less than 10 GeV, whereas the partially contained  $\mu$ -like events and the  $e$ -like events are caused by neutrinos whose energies range upto 100 GeV (figures 2(d) and 2(f) of Ref. [5]). Therefore in calculating the number of fully contained  $\mu$ -like events, we integrate over the neutrino energies only upto 10 GeV, whereas for  $e$ -like events and partially contained  $\mu$ -like events, we integrate over neutrino energies upto 100 GeV.

We need to make an assumption to calculate the Monte Carlo expectations for  $N_\mu^i$  and  $N_e^i$ . The detector acceptance in general is a complicated function of energy and is different for electrons and muons. Since we do not know these acceptances, we make a very simple assumption about them, namely that the acceptance for all fully contained events, for both electrons and muons, is the same and is independent of energy. We also assume that the acceptance for all the partially contained muon events is independent of energy. These assumptions are somewhat crude but they are the best one can do due to our lack of knowledge of the detector details.

We define the number of expected  $\mu$ -like and  $e$ -like events in bin  $i$ , in the absence of neutrino oscillations, to be

$$N_\mu^i|_{MC} = pN_\mu^i|_{N.O.}(FC) + qN_\mu^i|_{N.O.}(PC) \quad (22)$$

$$N_e^i|_{MC} = pN_e^i|_{N.O.}(FC) \quad (23)$$

In the above equations, the number for fully contained  $\mu$ -like events is obtained by doing the energy integration in the expression for  $N_\mu^i|_{N.O.}$  on the right hand side (rhs) of eq.(20) from  $E = 1.6$  GeV to  $E = 10$  GeV. The numbers for the partially contained  $\mu$ -like events and fully contained  $e$ -like events are obtained by doing the energy integration in the respective

expressions for  $N_\mu^i|_{N.O.}$  and  $N_e^i|_{N.O.}$  (rhs of eq.(20) and eq.(21)) from  $E = 1.6 \text{ GeV}$  to  $E = 100 \text{ GeV}$ . The numbers  $p$  and  $q$  are the detection efficiencies for fully contained and partially contained events, which we assumed are independent of energy. The ratios  $r_{MC}^i$  are now equal to

$$r_{MC}^i = \frac{N_\mu^i|_{N.O.}(FC) + f N_\mu^i|_{N.O.}(PC)}{N_e^i|_{N.O.}(FC)} \quad (24)$$

where  $f = q/p$ . We calculated the values of  $N_\mu^i|_{N.O.}(FC)$ ,  $N_\mu^i|_{N.O.}(PC)$  and  $N_e^i|_{N.O.}(FC)$  for all the five bins and tried to find a value of  $f$  such that eq.(24) reproduces the values of all five  $r_{MC}^i$ . We found that, for  $f = 0.13$ , values of  $r_{MC}^i$  yielded by eq.(24) are within 10% of the numbers listed in Table I. Hence we set  $f = 0.13$  in our calculation.

In the presence of oscillations, the number of  $\mu$ -like and  $e$ -like events are given by

$$N_\mu^i|_{W.O.} = \int \phi_{\nu_\mu}^i P_{\mu\mu} \sigma_\mu dE + \int \phi_{\bar{\nu}_\mu}^i P_{\bar{\mu}\bar{\mu}} \sigma_{\bar{\mu}} dE + \int \phi_{\nu_e}^i P_{e\mu} \sigma_\mu dE + \int \phi_{\bar{\nu}_e}^i P_{\bar{e}\bar{\mu}} \sigma_{\bar{\mu}} dE \quad (25)$$

$$N_e^i|_{W.O.} = \int \phi_{\nu_e}^i P_{ee} \sigma_e dE + \int \phi_{\bar{\nu}_e}^i P_{\bar{e}\bar{e}} \sigma_{\bar{e}} dE + \int \phi_{\nu_\mu}^i P_{\mu e} \sigma_e dE + \int \phi_{\bar{\nu}_\mu}^i P_{\bar{\mu}\bar{e}} \sigma_{\bar{e}} dE \quad (26)$$

where  $P_{\alpha\beta}$ s are the probabilities for neutrino of flavor  $\alpha$  to oscillate into flavor  $\beta$ , derived in the last section. These oscillation probabilities are functions of the distance of travel  $d$ , the mixing angles  $\phi$  and  $\psi$ , the mass difference  $\delta_{31}$  and the matter term  $A$ . These are calculated using the formulae in eqs. (8), (9), (10) and (14). The probability of oscillation for anti-neutrinos  $P_{\bar{\alpha}\bar{\beta}}$  is different from  $P_{\alpha\beta}$  because of the different  $A$  dependence. We define the predicted number of  $\mu$ -like and  $e$ -like events, in the presence of neutrino oscillations to be

$$N_\mu^i|_{pre} = p N_\mu^i|_{W.O.}(FC) + q N_\mu^i|_{W.O.}(PC) \quad (27)$$

$$N_e^i|_{pre} = p N_e^i|_{W.O.}(FC). \quad (28)$$

The limits for the energy integration in eqs.(25) and (26), in the calculation of  $N_\mu^i|_{W.O.}(FC)$ ,  $N_\mu^i|_{W.O.}(PC)$  and  $N_e^i|_{W.O.}(FC)$ , are the same as those in the corresponding terms for the case of no oscillations. The ratio of the predicted number of  $\mu$ -like and  $e$ -like events, in the presence of oscillations, is given by

$$r_{pre}^i = \frac{N_\mu^i|_{W.O.}(FC) + f N_\mu^i|_{W.O.}(PC)}{N_e^i|_{W.O.}(FC)} \quad (29)$$

where  $f = 0.13$ , as in the case of no oscillations. We define the ratio of the above ratio to the ratio of the Monte Carlo expectation

$$R_{pre}^i = \frac{r_{pre}^i}{r_{MC}^i}. \quad (30)$$

If the atmospheric neutrino deficit is due to neutrino oscillations, then the double ratios  $R_{pre}^i$  given in eq. (30) should be within the range of the corresponding observed double ratios  $R_{obs}^i$ , which are given in Table I. We searched for the values of the neutrino parameters  $\phi, \psi$  and  $\delta_{31}$  for which the predicted values of  $R_{pre}^i$  satisfy the experimental constraints on the double ratios for all the five bins. The ranges of variation in the three parameters are

1.  $0 \leq \phi \leq 40^0$ . This is the range of  $\phi$  allowed by the solar neutrino problem. For this range of  $\phi$ , there exist values of  $\delta_{21}$  and  $\omega$  such that all the three solar neutrino experiments can be explained [13,20].
2.  $0 \leq \psi \leq 90^0$ .  $\psi$  is varied over its fully allowed range.
3.  $10^{-3} \text{ eV}^2 \leq \delta_{31} \leq 10^{-1} \text{ eV}^2$ . The lower limit is given by the sub-GeV data and the upper limit is the largest value allowed by the two flavor analysis of the multi-GeV data by Kamiokande [5].

The results are plotted in Figures 2, 3 and 4. Figure 2 gives the projection of the allowed region on the  $\phi - \psi$  plane, Figure 3 gives the projection on the  $\phi - \delta_{31}$  plane and Figure 4 gives the projection on the  $\psi - \delta_{31}$  plane. The solid lines enclose the regions of parameter space whose predictions lie within the experimental range given by  $1\sigma$  uncertainties. The broken lines enclose regions whose predictions fall within range given by  $1.6\sigma$  uncertainties.

As seen from Table I, the uncertainties in bin 5, which has  $\langle \cos \theta \rangle = 0.8$ , are quite large compared to the uncertainties in the other four bins. Moreover,  $r_{obs}^5$  is greater than  $r_{MC}^5$  through most of its range. Hence the double ratio  $R_{obs}^5 > 1$  for most of its range. The Monte Carlo expectation of the electron neutrino flux is less than that of the muon neutrino flux

and the oscillation probabilities  $P_{\alpha\beta}$  are all less than 1. Using these facts, one can show from eqs. (24) and (29) that, in general,  $r_{pre}^i \leq r_{MC}^i$  or  $R_{pre}^i \leq 1$ . Therefore, the region of overlap between  $R_{obs}^5$  and  $R_{pre}^5$  is very small. It is  $0.9 - 1.0$  for  $1\sigma$  uncertainties. This small overlap places a very strong constraint on the allowed regions of the parameter space and is probably responsible for the very small allowed range of  $\delta_{31}$  seen in Figures 3 and 4 ( $0.015 \text{ eV}^2 \leq \delta_{31} \leq 0.025 \text{ eV}^2$ ). Thus it happens that the bin with the largest uncertainty is imposing the strongest constraint on the allowed values of the parameters. Because of this unsatisfactory situation, we redid the analysis ignoring the constraint from bin 5. We searched for regions of parameter space for which the values of  $R_{pre}^i$  are within the ranges of corresponding  $R_{obs}^i$  for only the first four bins.

The results of the 4 bin analysis are plotted in Figures 5, 6 and 7. Figure 5 gives the projection of the allowed region on the  $\phi - \psi$  plane, Figure 6 gives the projection on the  $\phi - \delta_{31}$  plane and Figure 7 gives the projection on the  $\psi - \delta_{31}$  plane. As before, the solid lines enclose the regions satisfying  $1\sigma$  vetoes and the broken lines enclose regions allowed by  $1.6\sigma$  vetoes. Comparing Figures 2 and 5, we see that the allowed region in the  $\phi - \psi$  plane is more or less unchanged both for  $1\sigma$  vetoes and  $1.6\sigma$  vetoes. However, in the case of  $\delta_{31}$ , the allowed range for  $1\sigma$  vetoes is greatly expanded to  $0.015 \text{ eV}^2 \leq \delta_{31} \leq 0.15 \text{ eV}^2$ . Note that the minimum allowed value is unchanged but the maximum allowed value for the 4 bin analysis is almost an order of magnitude larger than the corresponding value for the 5 bin analysis. In the case of  $1.6\sigma$  vetoes, the maximum allowed value of  $\delta_{31}$  can be as high as  $6 \text{ eV}^2$ , again much larger than the corresponding value for the 5 bin analysis.

#### IV. DISCUSSION AND CONCLUSIONS

The salient features of the results of the multi-GeV analysis are:

- Most of the parameter space allowed by the multi-GeV data is a subset of the space allowed by the sub-GeV data.

- The range of  $\delta_{31}$  allowed at  $1\sigma$  level is extremely narrow in the 5 bin analysis. It is very close to the best fit value given by the two flavor analysis of Kamiokande. The range of  $\delta_{31}$  allowed by the  $1.6\sigma$  vetoes in the 5 bin analysis is very similar to the region obtained by Kamiokande under similar constraints [5].
- The allowed range of  $\delta_{31}$  is much larger for the 4 bin analysis compared to the 5 bin analysis.
- The value of  $\psi$  is always large ( $\psi \geq 40^0$ ) and  $\psi = 90^0$  is allowed.
- In the region allowed by  $1\sigma$  vetoes,  $\phi$  is always non-zero.  $\phi = 0$  is allowed only at  $1.6\sigma$  level.

The parameter space shown in Figures 1 to 7 , together with the allowed values for  $\omega$  and  $\delta_{21}$  from our earlier work [13], provides a complete solution to the solar and the atmospheric neutrino problems in the framework of three flavor neutrino oscillations. The similarity between the allowed range of  $\delta_{31}$  in our analysis and the allowed range of the mass difference in Kamiokande's two flavor analysis indicates that the approximation made regarding the detector acceptances did not play a crucial role in determining the parameter space. This probably occurred due to the cancellation of the effects of the approximation in the numerator and the denominator of eq. (29).

From the parametrization of  $U^v$ , effective two level mixings can be obtained for the following choices of the angles:

- $\nu_e \leftrightarrow \nu_\mu$  for  $\psi = 90^0$ ,
- $\nu_e \leftrightarrow \nu_\tau$  for  $\psi = 0$  and
- $\nu_\mu \leftrightarrow \nu_\tau$  for  $\phi = 0$ .

Any solution to the atmospheric neutrino problem should suppress the muon neutrinos, enhance the electron neutrinos or do both. The  $\nu_e \leftrightarrow \nu_\tau$  channel, which suppresses electron neutrinos but leaves muon neutrinos untouched, cannot account for the atmospheric neutrino

problem. Hence any solution of atmospheric neutrino problem should be away from the effective two flavor  $\nu_e \leftrightarrow \nu_\tau$  oscillations. The large value of the angle  $\psi$  is just a reflection of this fact.

Matter effects can account for the zenith angle dependence of the multi-GeV data if they are important for the relevant energy range. There are no matter effects present for the  $\nu_\mu \leftrightarrow \nu_\tau$  channel. Hence any solution which takes into account the zenith angle dependence should disfavour this channel. That is, the solution should not pick out very small values the angle  $\phi$ . The zenith angle dependence of the multi-GeV data is present only if one limits the experimental uncertainties to  $1\sigma$  level. For  $1\sigma$  vetoes, we have a lower limit  $\phi \geq 8^0$ . If one considers  $1.6\sigma$  error bars, then it is possible to explain the multi-GeV data in terms of zenith angle independent neutrino oscillations. Thus  $\phi = 0$  (pure  $\nu_\mu \leftrightarrow \nu_\tau$  oscillation) is indeed included in the region allowed by  $1.6\sigma$  vetoes.

For the smallest values of  $\phi$  allowed by the  $1\sigma$  vetoes and  $\psi \sim 45^0$ , the solar neutrino problem is solved through  $\nu_e \rightarrow \nu_\mu$  oscillation, which is controlled by  $\delta_{21}$  and  $\omega$ , whereas the atmospheric neutrino problem is solved mostly by  $\nu_\mu \rightarrow \nu_\tau$  oscillation, which is controlled by  $\delta_{31}$  and  $\psi$ . However,  $\nu_\mu \rightarrow (\nu_1, \nu_3) \rightarrow \nu_e$  oscillation in this case is non-negligible and this provides the necessary zenith angle dependence needed to explain the multi-GeV data. For larger values of  $\phi$  ( $\phi \sim 30^0$  and  $\psi \sim 45^0$ ), there are two channels for  $\nu_e \leftrightarrow \nu_\mu, \nu_\tau$  oscillations. In one channel the intermediate states are the mass eigenstates  $\nu_1$  and  $\nu_2$ . This channel is controlled by  $\delta_{21}$  and it solves the solar neutrino problem. In the second channel the intermediate states are  $\nu_1$  and  $\nu_3$ , which is controlled by  $\delta_{31}$ . This provides the zenith angle dependent suppression of the atmospheric muon neutrinos. In addition  $\nu_\mu \rightarrow \nu_\tau$  oscillations are also allowed for these values of the mixing angles, which again are controlled by  $\delta_{31}$ . They partially account for the suppression of atmospheric muon neutrinos.

The allowed region includes the value  $\psi = 90^0$ . Then the atmospheric neutrino problem is explained purely in terms of the two flavor oscillations between  $\nu_e \leftrightarrow \nu_\mu$ , with the relevant mass difference being  $\delta_{31}$ . In this case, the solar neutrino problem is solved by  $\nu_e \rightarrow \nu_\tau$  oscillation which is determined by the mass difference  $\delta_{21}$  (and the mixing angles  $\omega$  and  $\phi$ ).

We now make a brief comment on the LSND results on the search for  $\bar{\nu}_\mu \rightarrow \bar{\nu}_e$  oscillations [15] in the context of our analysis of atmospheric neutrinos. The LSND collaboration gives an oscillation probability  $P_{\bar{\mu}e} = (3.1^{+1.1}_{-1.0} \pm 0.5) \times 10^{-3}$  for muon anti-neutrinos in the energy range 20 – 60 MeV. In the framework described in section II, the oscillation probability relevant for the LSND experiment is the vacuum oscillation probability

$$P_{\bar{\mu}e}^0 = P_{\mu e}^0 = \sin^2 2\phi \sin^2 \psi \sin^2 \left( 1.27 \frac{d \delta_{31}}{E} \right). \quad (31)$$

Note that both  $\phi$  and  $\psi$  have to be non-zero for  $P_{\mu e}$  to be non-zero. In the region allowed by the  $1\sigma$  vetoes of the multi-GeV atmospheric neutrino data (both for 4 bin and 5 bin analyses), we have

$$\begin{aligned} \text{Minimum } (\sin^2 2\phi \sin^2 \psi) &\simeq 0.04 \text{ for } \phi \simeq 8^0, \psi \simeq 40^0 \\ \text{Maximum } (\sin^2 2\phi \sin^2 \psi) &\simeq 1 \text{ for } \phi \simeq 40^0, \psi \simeq 90^0. \end{aligned}$$

Substituting these values and the oscillation probability obtained by LSND in eq. (31), we obtain

$$0.001 \leq \sin^2 \left( 1.27 \frac{d \delta_{31}}{E} \right) \leq 0.1. \quad (32)$$

For the LSND experiment the distance  $d = 30$  meters. Taking the average energy to be  $\langle E \rangle = 40$  MeV, we obtain the range of  $\delta_{31}$  to be

$$0.03 \text{ eV}^2 \leq \delta_{31} \leq 0.3 \text{ eV}^2. \quad (33)$$

There is a significant overlap between this range and the range of  $\delta_{31}$  allowed by the  $1\sigma$  vetoes of the 4-bin analysis, ( $0.015 \text{ eV}^2 \leq \delta_{31} \leq 0.15 \text{ eV}^2$ ), shown in Figures 6 and 7. If one considers the region allowed by  $1.6\sigma$  vetoes of the multi-GeV data, both in the 4 bin and 5 bin analyses, then the lower limit on  $\phi$  disappears and  $\phi$  is allowed to be arbitrarily small. From eq. (31) we see that, for small values of  $\phi$ ,  $\delta_{31}$  can be quite large. In this case, there is a very large region of overlap in the range of  $\delta_{31}$  allowed by the LSND result and the 4 bin analysis of the multi-GeV data. This suggests that the standard three flavor analysis can accomodate all data so far and perhaps a fourth sterile neutrino is not needed.

In conclusion, we have analyzed the atmospheric neutrino data of Kamiokande in the context of three flavor neutrino oscillations. We took into account both the zenith angle dependence of the multi-GeV data and the matter effects due to the propagation of the neutrinos through the earth. We obtained the regions in neutrino parameters which solve both the solar and the atmospheric neutrino problems. If we require that the constraints from all the 5 zenith angles bins should be satisfied, the allowed range of  $\delta_{31}$  is quite small. If we relax the constraint from the 5th bin, which has the largest uncertainties, a much larger range of  $\delta_{31}$  is allowed. Earth matter effects can explain the zenith angle dependence of the multi-GeV data. If one considers  $1\sigma$  uncertainties, then  $\phi$  has a lower limit  $\phi \geq 8^0$ . The mixing angle  $\psi$  is constrained to be large,  $\psi \geq 40^0$ .

**Acknowledgements:** We are grateful to M. V. N. Murthy for collaboration during the earlier part of this work and for a critical reading of the manuscript. We also thank S. R. Dugad and Rahul Sinha for numerous discussions during the course of this work.

## REFERENCES

- [1] M. Honda *et al*, Phys. Rev. **D52**, 4985 (1995).
- [2] V. Agrawal *et al*, Phys. Rev. **D53**, 1314 (1996).
- [3] D. Casper *et al.*, Phys.Rev.Lett. **66**, 2561(1991); R. Becker-Szendy *et al.*, Phys. Rev. **D 46**, 3720(1992).
- [4] Kamiokande Collaboration: K. S. Hirata *et al*, Phys. Lett. **B280**, 146 (1992).
- [5] Kamiokande Collaboration: Y. Fukuda *et al*, Phys. Lett. **B335**, 237 (1994).
- [6] J. Pantaleone, Phys. Rev. **D49**, R2152 (1994).
- [7] S. Goswami, K. Kar and A. Raychaudhury, CUPP-95/3 May 1995, hep-ph/9505395; S. Goswami, CUPP-95/4 July 1995, hep-ph/9507212.
- [8] S. M. Bilenky, C. Giunti and C. W. Kim, hep-ph 9505301.
- [9] C. Giunti, C. W. Kim and J. D. Kim, Phys. Lett. **352B**, 357 (1995).
- [10] D. Harley, T. K. Kuo and J. Pantaleone, Phys. Rev. **D47**, 4059 (1993).
- [11] G. Fogli, E. Lisi and D. Montanino, Phys. Rev. **D49**, 3626 (1994); Astropart. Phys. **4**, 177 (1995).
- [12] A. S. Joshipura and P. I. Krastev, Phys. Rev. **D 50**, 3484 (1994).
- [13] M. Narayan *et al*, Phys. Rev. **D53**, 2809 (1996).
- [14] O. Yasuda, TMUP-HEL-9603 February 1996, hep-ph/9602342
- [15] LSND Collaboration: C. Athanassopoulos *et al*, Los Alamos Preprint LA-UR-96-1582, nucl-ex/9605003.
- [16] L. Wolfenstein, Phys. Rev. **D17**, 2369 (1978); **D20**, 2634 (1979).
- [17] We thank J. Pantaleone for pointing this out to us.

- [18] T. K. Gaisser and J. S. O'Connell, Phys. Rev **D34**, 822 (1986).
- [19] P. Musset and J. P. Vialle, Phys. Rep. **39C**, 1 (1978).
- [20] G. L. Fogli, E. Lisi and D. Montanino, Institute for Advanced Study Report No. IASSNS-AST/96-21, hep-ph/9605273, to appear in Phys. Rev. D.

## TABLES

Bin No.	$\langle \cos\theta \rangle$	$\langle \text{distance} \rangle$ in Km	$r_{MC}^i$	$r_{obs}^i$	$R_{obs}^i$
1	-0.8	10,210	3.0	$0.87^{+0.36}_{-0.21}$	$0.29^{+0.12}_{-0.07}$
2	-0.4	5,137	2.3	$1.06^{+0.39}_{-0.30}$	$0.46^{+0.17}_{-0.13}$
3	0.0	832	2.1	$1.07^{+0.32}_{-0.23}$	$0.51^{+0.15}_{-0.11}$
4	0.4	34	2.3	$1.45^{+0.51}_{-0.34}$	$0.63^{+0.22}_{-0.16}$
5	0.8	6	3.0	$3.9^{+1.8}_{-1.2}$	$1.3^{+0.6}_{-0.4}$

TABLE I. Zenith angle dependent data from Kamiokande [5]

## FIGURES

FIG. 1. Allowed region in  $\phi - \psi$  plane by the sub-GeV data (with  $\delta_{31} \geq 10^{-3} \text{ eV}^2$ ) at  $1\sigma$  (enclosed by solid lines) and at  $1.6\sigma$  (enclosed by broken lines)

FIG. 2. Allowed region in  $\phi - \psi$  plane by 5 bin analysis of multi-GeV data (with  $10^{-3} \text{ eV}^2 \leq \delta_{31} \leq 10^{-1} \text{ eV}^2$ ) at  $1\sigma$  (enclosed by solid lines) and at  $1.6\sigma$  (enclosed by broken lines)

FIG. 3. Allowed region in  $\phi - \delta_{31}$  plane by 5 bin analysis of multi-GeV data (with  $0 \leq \psi \leq 90^0$ ) at  $1\sigma$  (enclosed by solid lines) and at  $1.6\sigma$  (enclosed by broken lines)

FIG. 4. Allowed region in  $\psi - \delta_{31}$  plane by 5 bin analysis of multi-GeV data (with  $0 \leq \phi \leq 40^0$ ) at  $1\sigma$  (enclosed by solid lines) and at  $1.6\sigma$  (enclosed by broken lines)

FIG. 5. Allowed region in  $\phi - \psi$  plane by 4 bin analysis of multi-GeV data (with  $10^{-3} \text{ eV}^2 \leq \delta_{31} \leq 10 \text{ eV}^2$ ) at  $1\sigma$  (enclosed by solid lines) and at  $1.6\sigma$  (enclosed by broken lines)

FIG. 6. Allowed region in  $\phi - \delta_{31}$  plane by 4 bin analysis of multi-GeV data (with  $0 \leq \psi \leq 90^0$ ) at  $1\sigma$  (enclosed by solid lines) and at  $1.6\sigma$  (enclosed by broken lines)

FIG. 7. Allowed region in  $\psi - \delta_{31}$  plane by 4 bin analysis of multi-GeV data (with  $0 \leq \phi \leq 40^0$ ) at  $1\sigma$  (enclosed by solid lines) and at  $1.6\sigma$  (enclosed by broken lines)

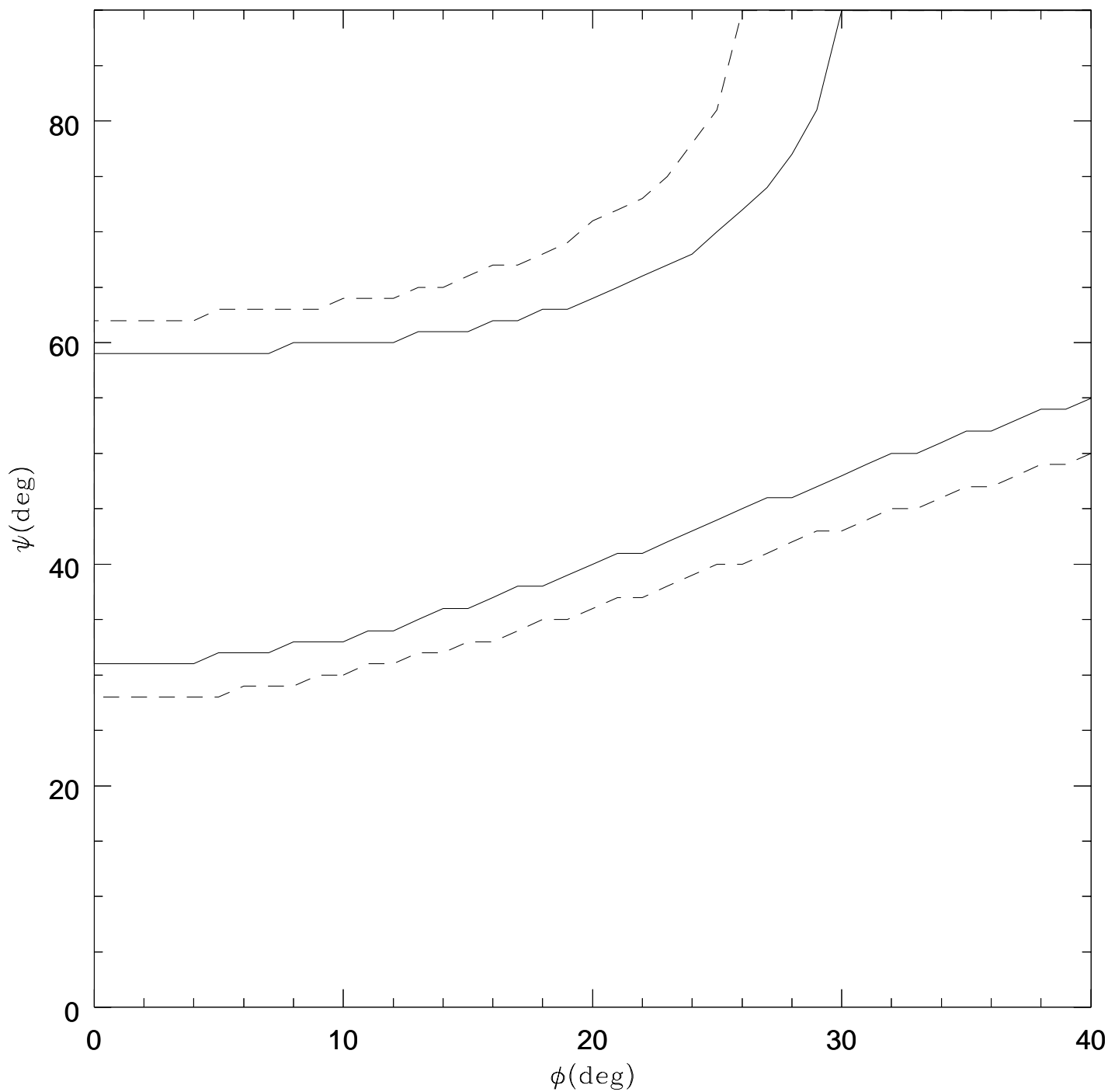


Fig1

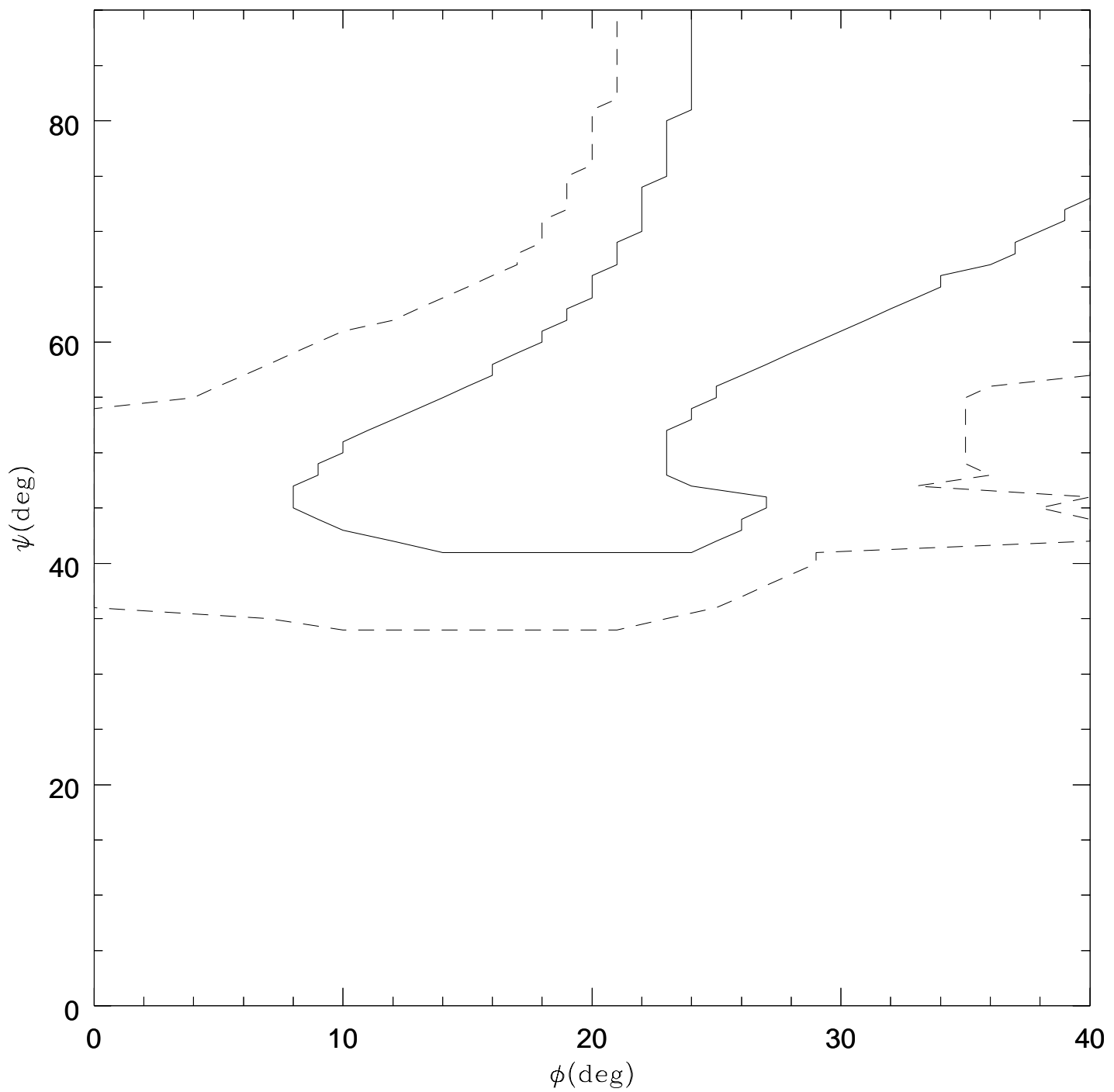


Fig2

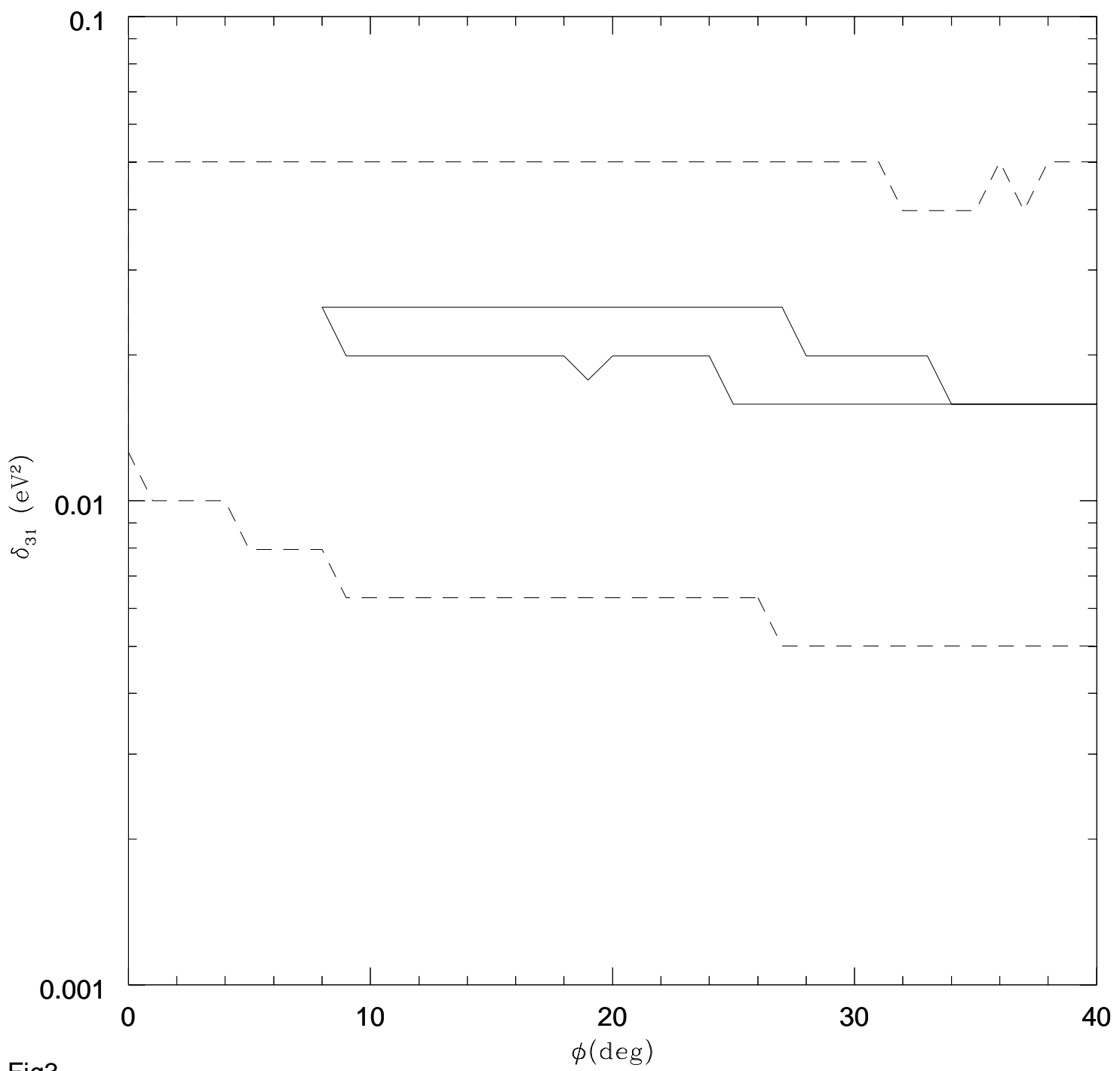


Fig3

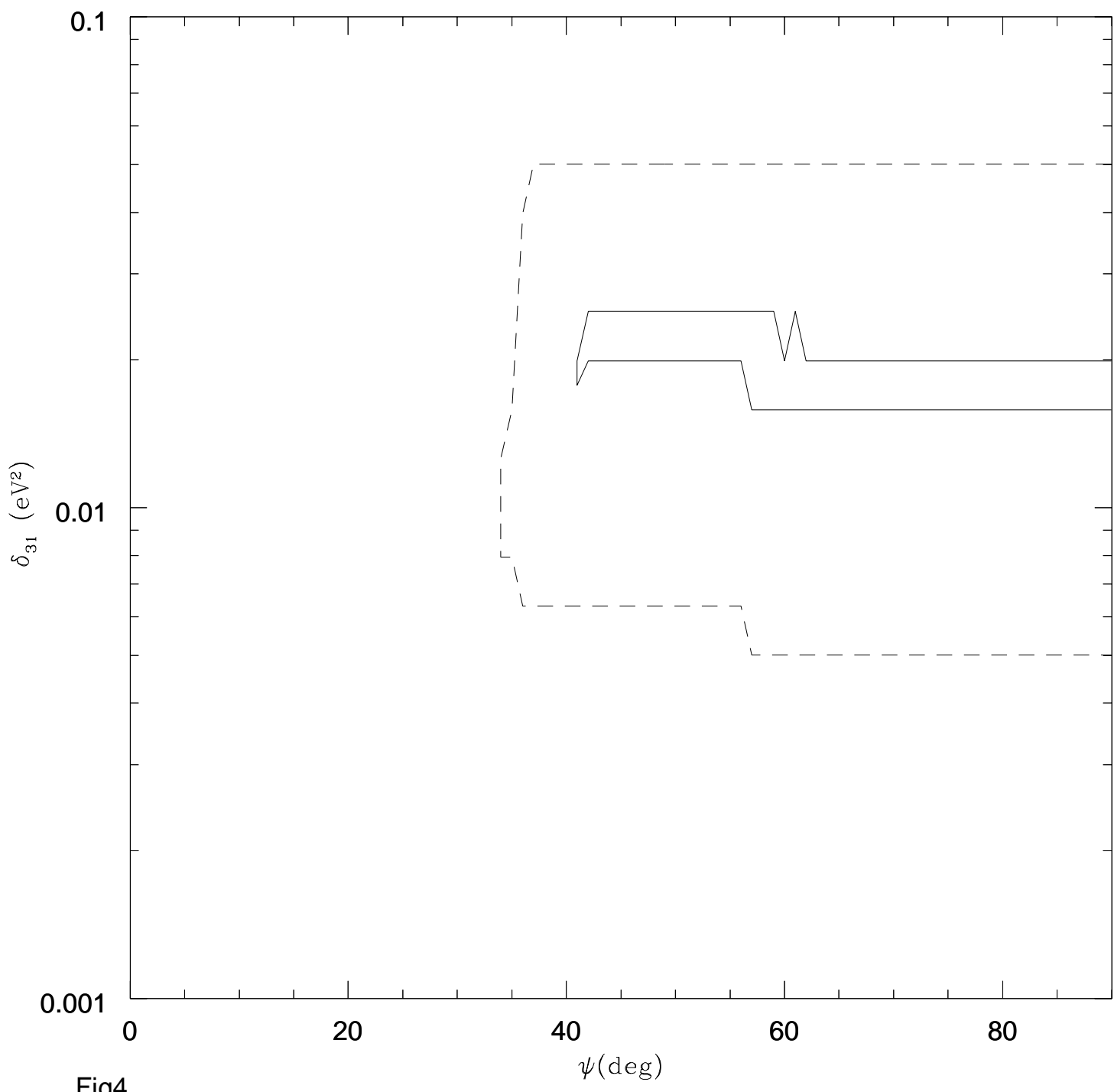


Fig4

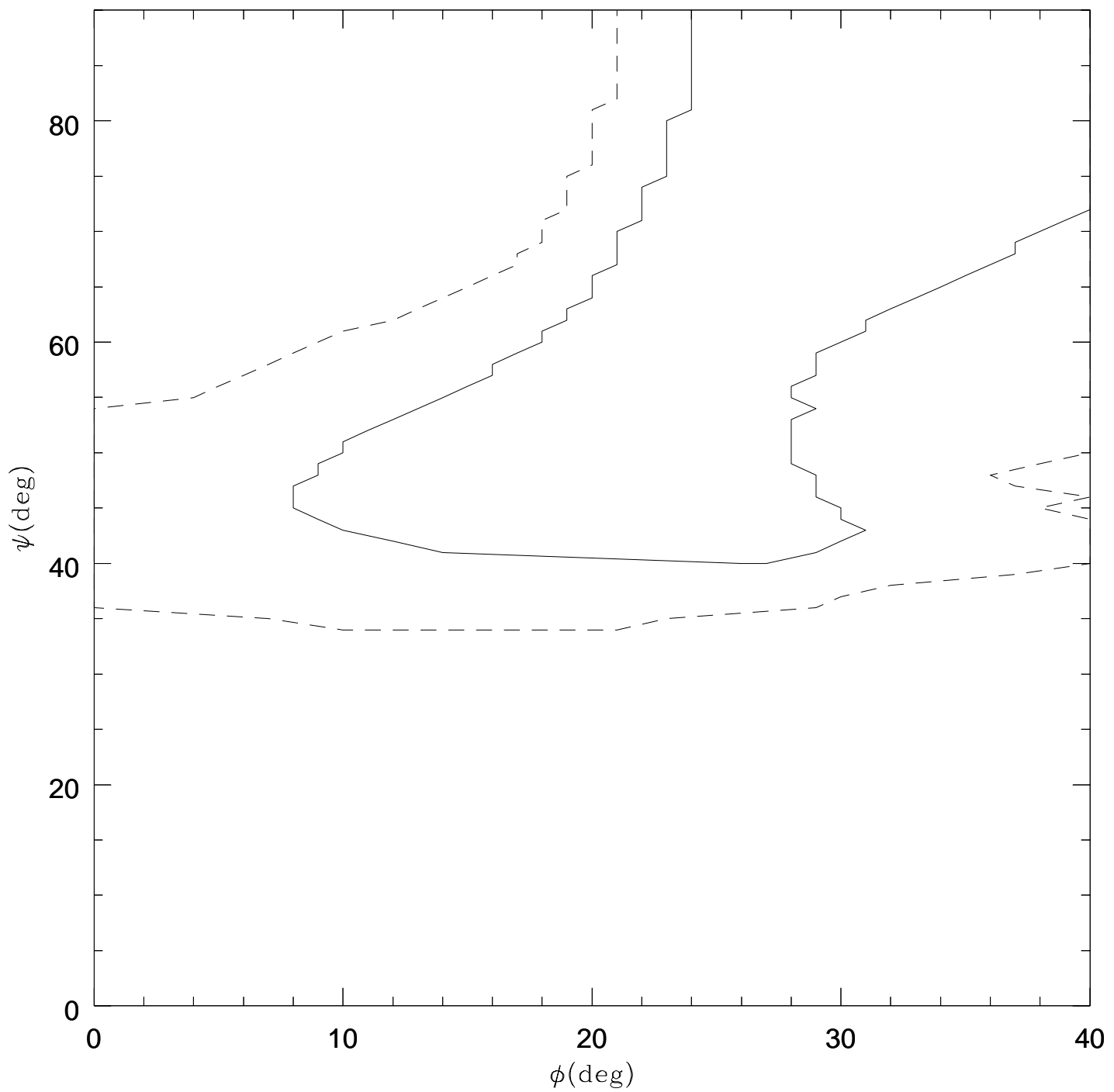


Fig5

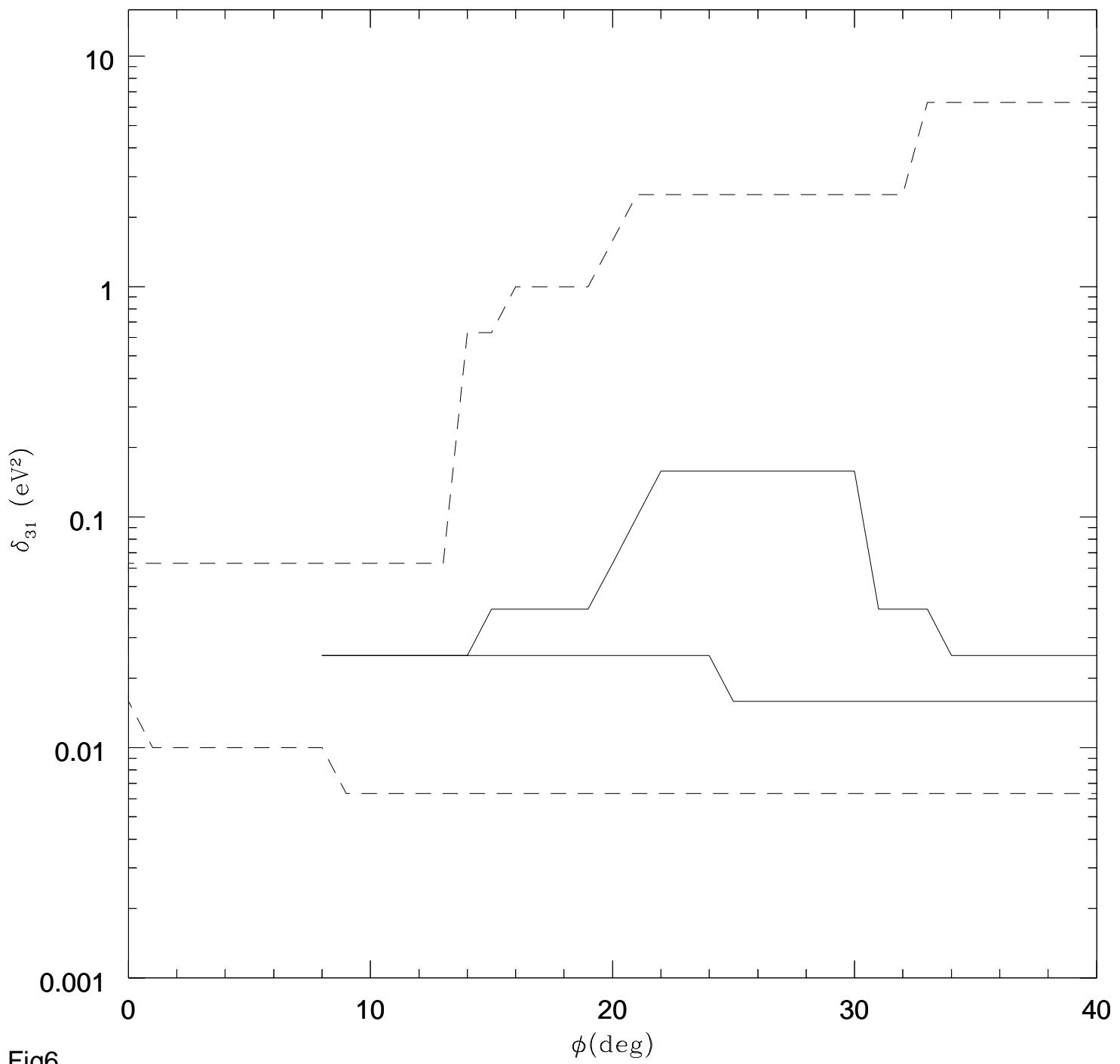


Fig6

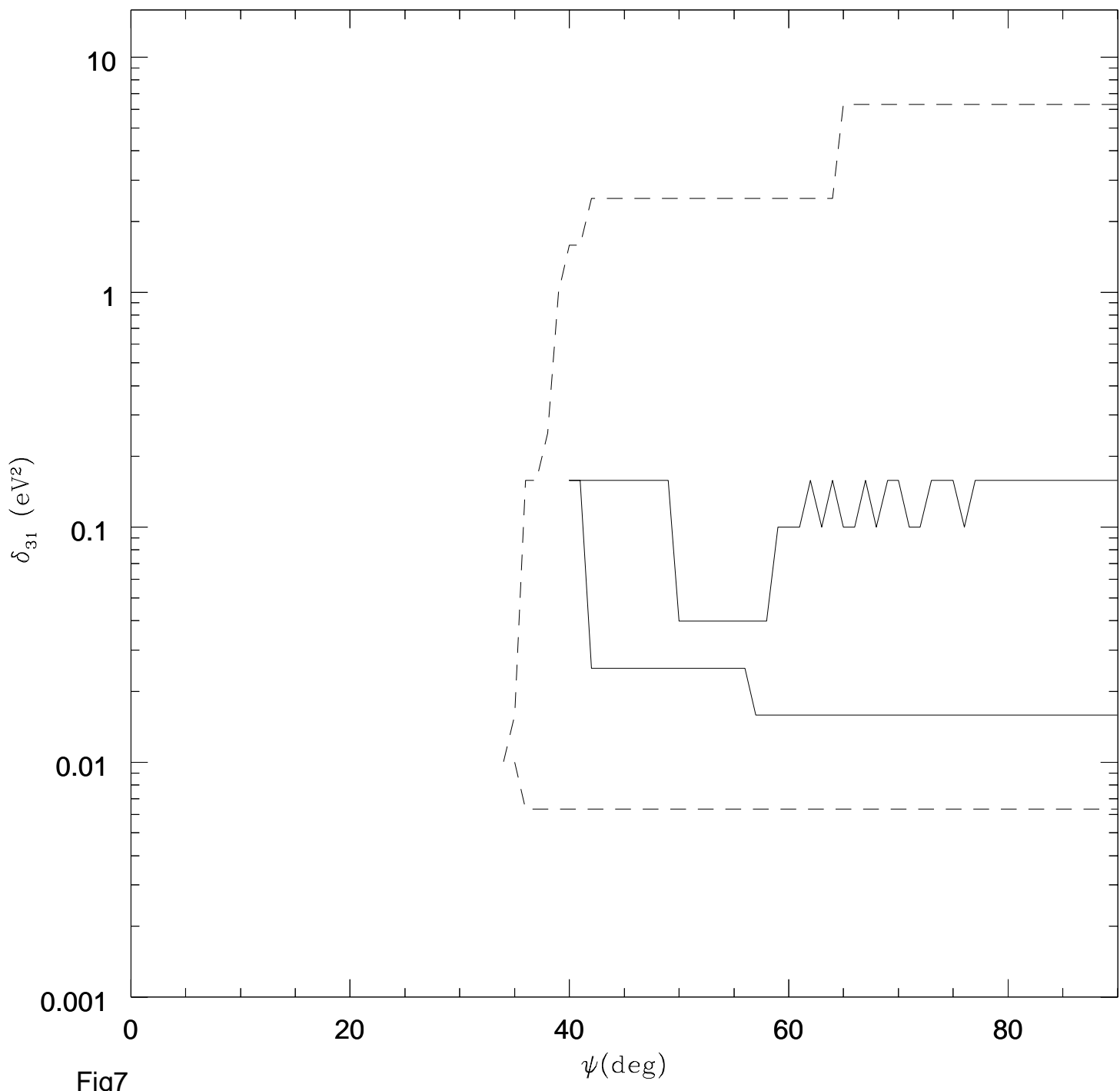


Fig7